

## Supporting Information

### Multi-functional biomimetic graphene induced transformation of $\text{Fe}_3\text{O}_4$ to $\epsilon\text{-Fe}_2\text{O}_3$ at room temperature

Soumya Bhattacharya<sup>a</sup>, Anirban Roychowdhury<sup>b,c</sup>, Dipankar Das<sup>b</sup> and Suprabha Nayar<sup>a</sup>

<sup>a</sup>Material Science and Technology Division, CSIR-National Metallurgical Laboratory, Jamshedpur - 831007, India

<sup>b</sup>UGC-DAE Consortium for Scientific Research, III/LB-8, Bidhannagar, Kolkata-700098, India

<sup>c</sup>Department of Physics, Krishnath College, Berhampore-742101, West Bengal, India

#### SI-1. Fourier Transform Infrared Spectroscopy

The FTIR spectrum is complex showing signatures of proteins/polymers, graphene and iron oxide. All the obtained peaks are assigned to bonds in the Table, the peak at  $850\text{cm}^{-1}$  provides direct evidence that iron has actually interacted with the functionalized graphene.

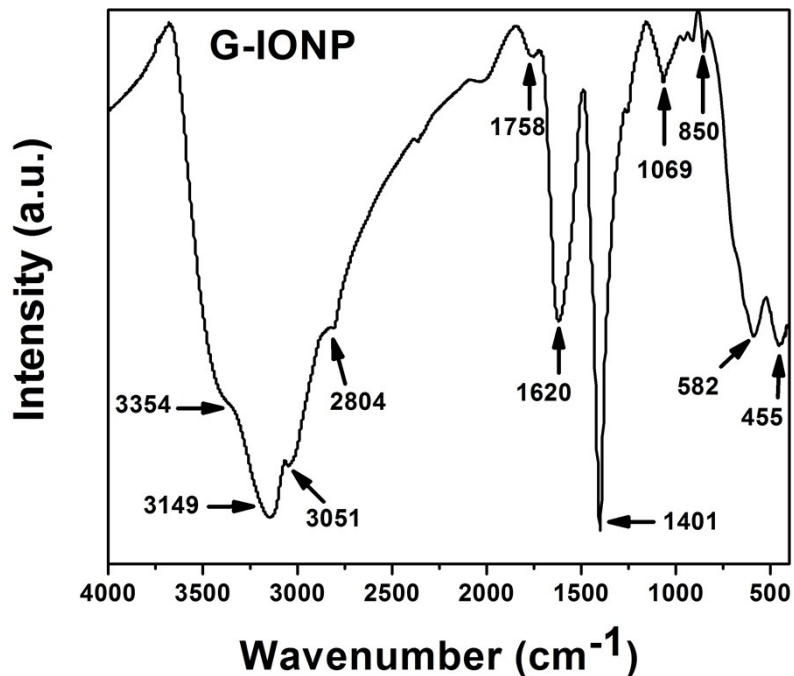


**Fig. S1.** The FTIR spectra of the composites.

**Table S1.** Vibrational frequencies of functional groups and bonds in G-IONP composites.

Wavenumber (cm <sup>-1</sup> )	Bond Assignments
3354	OH stretching for water molecules
3149	N-H stretching/ OH stretching for carboxyl groups
3051	C=C-H asymmetric stretching of aromatic amino acids; vibrational ring modes due to symmetric stretching of NH <sub>2</sub> groups in proteins <sup>1</sup>
2804	C-H stretching of PVA molecule
1758	C=O stretching of carboxyl groups in acetic acid
1620,1401 & 1069	N-H bending vibrations in amino acid side chains such as proline and hydroxyproline present in Collagen and also in BSA <sup>2-3</sup>
850	Fe-N stretching <sup>4</sup>

582	Fe-O stretching <sup>5</sup>
455	Fe-O stretching <sup>5</sup>

## SI-2. Thermogravimetry and Differential Thermal Analysis

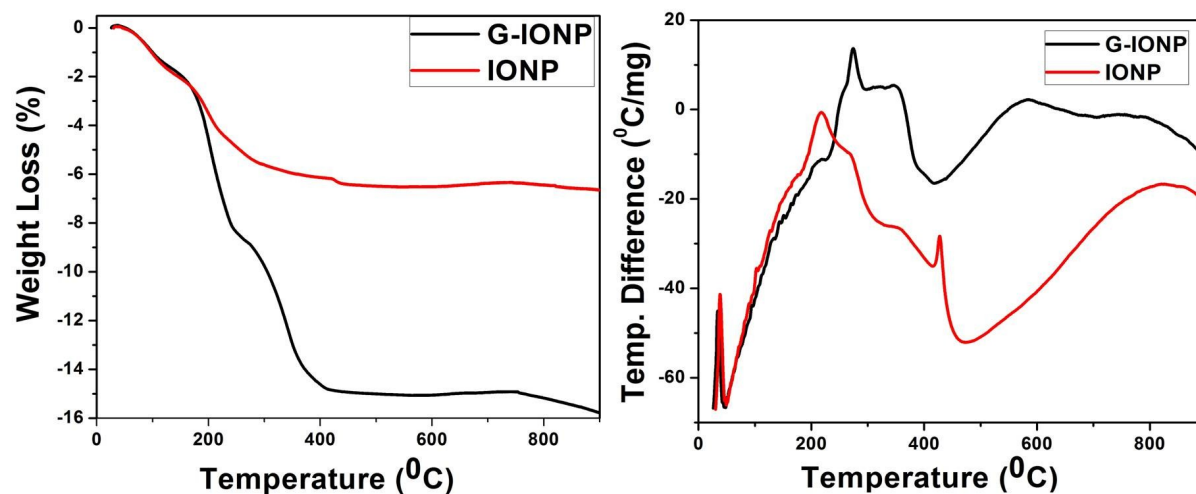


**Fig. S2.** (a) Thermogravimetry (TGA) and Differential Thermal Analysis (DTA) of the composites (G-IONP) and iron oxide nanoparticles (IONPs) without graphene.

Thermal analysis detects the physical properties of materials, its inter-atomic and inter-/intra molecular interactions as related to an imposed external change in temperature. In combination with other characterization techniques it provides unique information. In this study, TGA-DTA results were amongst the first to give a finger print of the presence of graphene, this difference was not expected as there is very little graphene in the system. The surface area of graphene must be attracting the ferric ions preferentially. From Fig. S2 we can see that a little below 200 to about 400° C, the mass change of G-IONP is significantly different from IONP. DTA measures

the temperature difference associated with phase transitions or reactions. Here again the shape of the two curves is significantly different, an indication of the phase composition change.

### **SI-3. Positron Annihilation Spectroscopy**

Positron annihilation spectroscopy (PAS) is the most important tool to study the material's defects as it has the versatility to explore the electronic environment around it. As the ratio of ferric/ferrous ions: graphene is 850:1, it was necessary to do lifetime spectroscopy to understand the environmental differences<sup>6</sup>. Apart from this, graphene sheet contains different types of defects which are produced naturally during synthesis. Three lifetime components  $\tau_1$ ,  $\tau_2$  and  $\tau_3$  with corresponding intensities  $I_1$ ,  $I_2$  and  $I_3$  are tabulated in Table-S3. The shortest lifetime component ( $\tau_1$ ) represents free annihilation due to free electrons residing at the grain boundaries or due to cation vacancies in the material.<sup>6</sup> Intermediate lifetime component ( $\tau_2$ ) indicates the free volumes around IONPs or interregional free spaces between the graphene sheet and IONPs. Lastly the third lifetime component ( $\tau_3$ ) originates from the pick-off annihilation due to larger vacancies or due to formation of ortho-positronium (o-Ps). It is clear from the table that the value of  $\tau_1$  for composite is lower and intensity higher compared to the graphene as expected since the delocalized graphene electrons annihilate faster. The reduction of  $\tau_2$  value and the subsequent increase of  $I_2$  for the composite indicates shrinkage of free volumes due to nucleation and growth of IONPs. Although the introduction of IONPs contributes to the shrinkage in the free volumes, but the number of intergrain cavities for the IONPs increase in the composite and this results a significant number of positrons getting trapped. This is the main cause of the increment of intensity value ( $I_2$ ) in the composite. Also, it is noted that the bigger lifetime component ( $\tau_3$ ) for

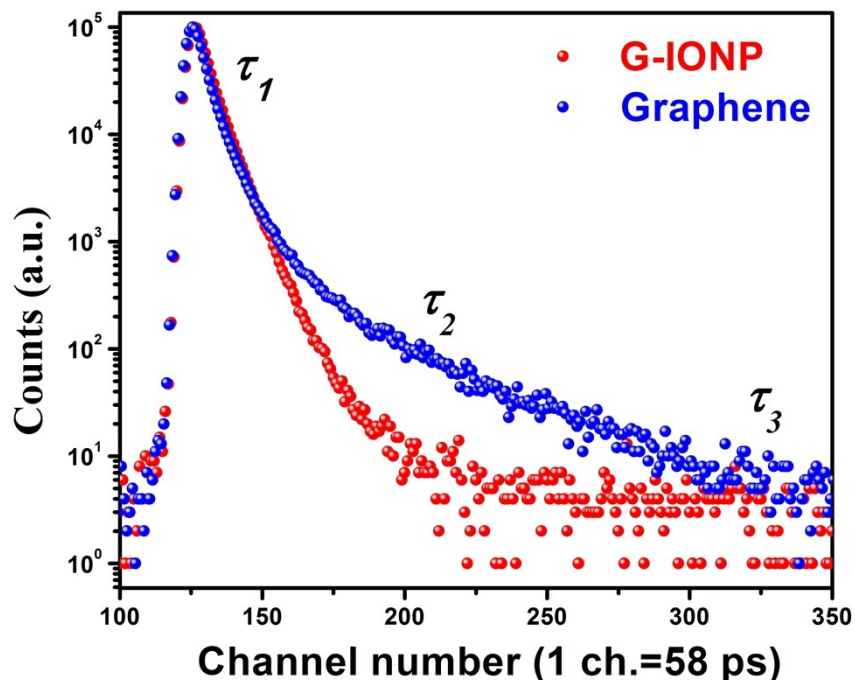


**Fig. S3.** Positron Annihilation Spectra showing a decrease in  $\tau_1$  and  $\tau_2$  lifetimes with an increase in  $\tau_3$  in G-IONP compared to IONP.

the composite shows very high value with very low intensity (<1%) suggesting that the vacancy clusters or larger free volumes were occupied by the IONP and chances of o-Ps formation reduces with respect to graphene. Lastly, the most reliable parameter, average positron annihilation lifetime component ( $\tau_{av}$ ) was calculated from the relation<sup>7</sup>

$$\tau_{av} = (\tau_1 I_1 + \tau_2 I_2 + \tau_3 I_3) / (I_1 + I_2 + I_3) = (\tau_1 I_1 + \tau_2 I_2 + \tau_3 I_3) / 100$$

Also, this average lifetime value decreases indicating the overall defects in the composite with respect to pure graphene which may play a vital role in its physical properties.

**Table-S3.** Positron annihilation lifetime parameters of the samples

Sample ID	$\tau_1$ (ns)	$\tau_2$ (ns)	$\tau_3$ (ns)	$I_1$	$I_2$	$I_3$	$\tau_m$ (ns)	$\chi^2$
<b>G-IONP</b>	0.1497	0.3487	3.4070	32.3408	67.5475	0.1117	0.2878	0.96
	$\pm 0.0051$	$\pm 0.0028$	$\pm 0.4331$	$\pm 1.5935$	$\pm 1.5892$	$\pm 0.0140$		
<b>Graphene</b>	0.1836	0.4185	2.0171	61.8865	34.0808	4.0327	0.3376	1.04
	$\pm 0.0035$	$\pm 0.0095$	$\pm 0.0301$	$\pm 1.8390$	$\pm 1.7723$	$\pm 0.1079$		

#### SI-4. SQUID Magnetometry

The room temperature hysteresis of IONPs showed the typical superparamagnetic behavior with a magnetic saturation,  $M_S$  of 12.52 emu/gm and negligible coercivity,  $H_C$  ( $\approx 20$  Oe) (Fig. S4). At 5K, below the blocked state, both the magnetization and coercivity increases; the values are greater than that of G-IONP, which proves graphene functionalization in the composites. Since there is not much difference in the particle size, the high magnetization can be attributed to the  $Fe_3O_4$  phase formed in the absence of graphene matrix. The M-T measurements (FC-ZFC curves, Fig. S4) showed an increase in the  $T_B$  from 27K in G-IONP to 36K in IONP; the increase is a sign of dipolar interactions in the sample which is reconfirmed from the dip in the FC curve below  $T_B$ , the plateau like feature, a sign of collective behavior. The particles in G-IONP being embedded in the graphene matrix are evenly distributed; the matrix prevents the particles to come in contact; the lower effective anisotropy value (see Table S4) means that the particles are able to relax more freely in the absence of graphene. The absence of exchange bias in IONPs proves that there is no formation of antiferro-ferrimagnetic exchange coupling in the sample which requires two different phases to be in contact.

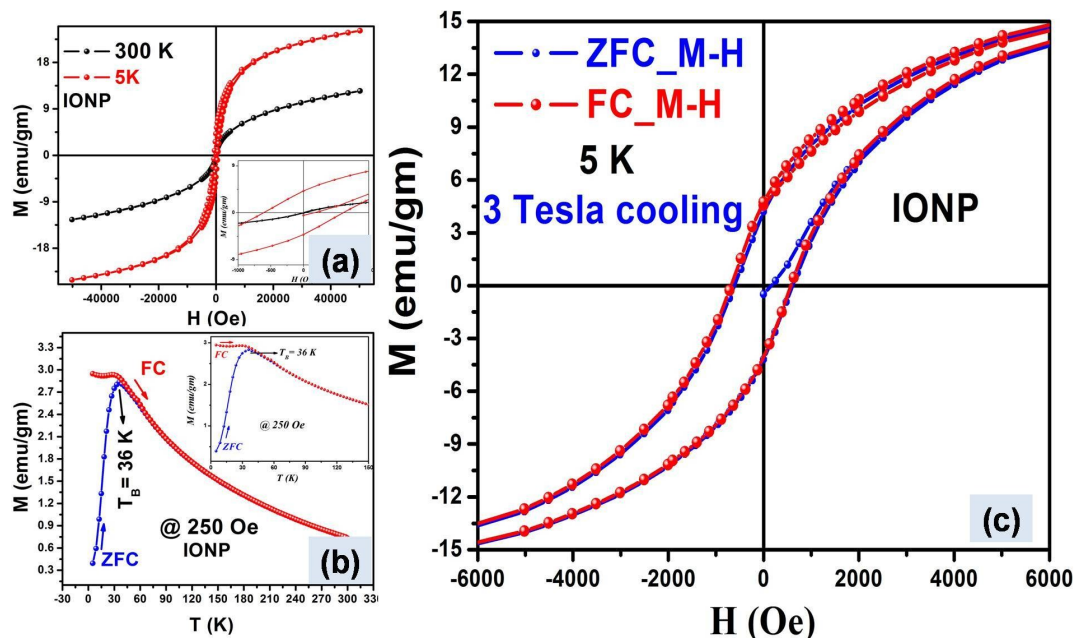


**Fig. S4.** (a) Room temperature hysteresis (M-H) showing superparamagnetic behavior, (b) The M-T curve showing blocking at 36K and (d) absence of exchange bias in the sample.

**Table S4.** Magnetic parameters of IONPs without graphene

Sample	Particle Size (nm)	Temp. (Kelvin)	$M_S^a$ (emu/gm)	$M_R^b$ (emu/gm)	$H_C^c$ (Oe)	$K_{eff}^d$ ( $\times 10^5$ erg/cc)	$T_B^e$ (Kelvin)
IONP	1.5	300K	12.52	0.073	20.00	732	36
		5K	24.20	4.185	617.42	-	-

## Notes and References

- 1 S. Srivastava, S. Srivastava, S. Srivastava, M. Shukla and V.D. Gupta, *J. Macromol. Sci. Part B: Phys.*, 2008, **47**, 654–666.
- 2 I.F. Spahr and J.T. Edsall, *J. Biol. Chem.*, 1964, **239**, 850-854.
- 3 A. Barth, *Prog. Biophys. Mol. Biol.*, 2000, **74**, 141-173.
- 4 E.J. Klinker, Ph.D. Thesis, The University of Minnesota, 2007.
- 5 R.M. Cornell and U. Schwertmann, in *The Iron Oxides: Structure, Properties, Reactions, Occurrences and Uses*, ed. R.M. Cornell and U. Schwertmann, Wiley-VCH Verlag GmbH & Co. Weinheim, 2nd edn., 2003.
- 6 U. Rana, P.M.G. Nambissan, S. Malika and K. Chakrabarti, *Phys. Chem. Chem. Phys.*, 2014, **16**, 3292-3298.
- 7 A. Roychowdhury, S.P. Pati, A.K. Mishra, S. Kumar and D. Das *J. Phys. Chem. Solids*, 2013, **74**, 811-813.